PHYSICAL REVIEW B **96**, 220401(R) (2017)

Quantum criticality of spinons

Feng He,[1,2] Yuzhu Jiang,[1] Yi-Cong Yu,[1,2] H.-Q. Lin,[3,*] and Xi-Wen Guan[1,4,5,†]

[1]*State Key Laboratory of Magnetic Resonance and Atomic and Molecular Physics, Wuhan Institute of Physics and Mathematics, Chinese Academy of Sciences, Wuhan 430071, China*

[2]*University of Chinese Academy of Sciences, Beijing 100049, China*

[3]*Beijing Computational Science Research Center, Beijing 100193, China*

[4]*Center for Cold Atom Physics, Chinese Academy of Sciences, Wuhan 430071, China*

[5]*Department of Theoretical Physics, Research School of Physics and Engineering, Australian National University, Canberra ACT 0200, Australia*

(Received 2 February 2017; revised manuscript received 16 November 2017; published 7 December 2017)

Magnon bound states emerging in one-dimensional (1D) spin chains still lack a rigorous understanding. In this Rapid Communication we show that the length-1 spin strings significantly dominate the critical properties of spinons, magnons, and free fermions in the 1D antiferromagnetic spin-1/2 chain. Using the Bethe ansatz solution, we analytically calculate the scaling functions of the thermal and magnetic properties of the model, providing a rigorous understanding of the quantum criticality of spinons. It turns out that the double maxima in specific heat elegantly mark two crossover temperatures fanning out from the critical point, indicating three quantum phases: the Tomonaga-Luttinger liquid (TLL), the quantum critical, and fully polarized ferromagnetic phases. For the TLL phase, the Wilson ratio $R_W = 4K_s$ remains almost temperature independent, where K_s is the Luttinger parameter. Furthermore, by applying our results, we precisely determine the quantum scalings and critical exponents of all magnetic properties in the ideal 1D spin-1/2 antiferromagnet $Cu(C_4H_4N_2)(NO_3)_2$, recently studied by Kono *et al.* [Phys. Rev. Lett. **114**, 037202 (2015)]. We further find that the magnetization maximum used in experiments is not a good quantity to map out the finite-temperature TLL phase boundary.

DOI: 10.1103/PhysRevB.96.220401

Of central importance to the study of the one-dimensional (1D) spin-1/2 antiferromagnetic Heisenberg chain is the understanding of spin excitations [1–13]. Elementary spin excitations in this model may exhibit quasiparticle behavior which is described by spinons carrying half a unit of spin. Such fractional quasiparticles are responsible for the Tomonaga-Luttinger liquid (TLL) and correlations in the model [14–20].

Regarding the Bethe ansatz (BA) solution of the 1D spin-1/2 chain, a significant development is Takahashi's discovery of spin string patterns [21], i.e., magnon bound states with different string lengths. Takahashi's spin strings give one full access to the thermodynamics of the model through Yang and Yang's grand canonical approach [22], namely, the so-called thermodynamic Bethe ansatz (TBA) equations [21]. However, the problems of how such spin strings determine the free-fermion nature of spinons and how spin strings comprise universal scalings of thermal and magnetic properties still lack a rigorous understanding. In this Rapid Communication we present an answer to these questions.

Using spin string solutions to the TBA equations, we obtain the following results: (I) We obtain exact scaling functions, critical exponents, and a benchmark of quantum magnetism for the 1D spin-1/2 Heisenberg chain, revealing the microscopic origin of the spinons and magnons that emerge in different physical regimes. (II) We find that the Wilson ratio (WR) [23,24], the ratio between the susceptibility χ and the specific heat c_v divided by the temperature T, $R_{\rm W} = \frac{4}{3}(\frac{\pi k_B}{g\mu_B})^2 \chi/(c_v/T)$, significantly characterizes the TLL of spinons and marks the crossover temperature between the quantum critical phase and the TLL [25] (see Fig. 1). We show that the specific heat maxima elegantly mark the phase boundaries between different phases at quantum criticality. When the magnetic field is larger than the saturation field, dilute magnon behavior is evidenced by the exponential decay of the susceptibility. (III) Using our results, we precisely determine the crossover temperatures, quantum scalings, and magnetic properties of the ideal spin-1/2 antiferromagnet $Cu(C_4H_4N_2)(NO_3)_2$ (hereafter referred to as CuPzN) [25]. We also find that the magnetization maximum used in experiments [25–28] is not a good quantity to map out the finite-temperature TLL phase boundary. Instead, one should use the WR or the specific heat maxima. Our results shed light on the criticality of spinons in systems with interacting charges and spins [29–32].

Bethe ansatz equations. The Hamiltonian of the 1D Heisenberg spin 1/2 chain is given by [33]

$$\mathcal{H} = 2J \sum_{j=1}^{N} \vec{S}_j \cdot \vec{S}_{j+1} - g\mu_B H M^z, \tag{1}$$

where J is the intrachain coupling constant, N is the number of lattice sites, and $M^z = \sum_{j=1}^{N} S_j^z = N/2 - M$ is the magnetization. M is the number of down spins. In this Hamiltonian, g and μ_B are the Landé factor and the Bohr magneton, respectively. To simplify the notation, we let $g\mu_B = 1$. The spin-1/2 operator $\vec{S}_j$ associated with the site j interacts with its nearest neighbors under a magnetic field H. The energy is given by $E = -\sum_{j=1}^{M} \frac{J}{\lambda_j^2 + \frac{1}{4}} + HM + E_0$, where $E_0 = \frac{1}{2}N(J - H)$, and the spin quasimomenta λ_j with $j = 1, \ldots, M$ are determined by the BA equations [5,33] (also see Ref. [34]). For the ground state, all the λ_j take real values.

*haiqing0@csrc.ac.cn

†xiwen.guan@anu.edu.au

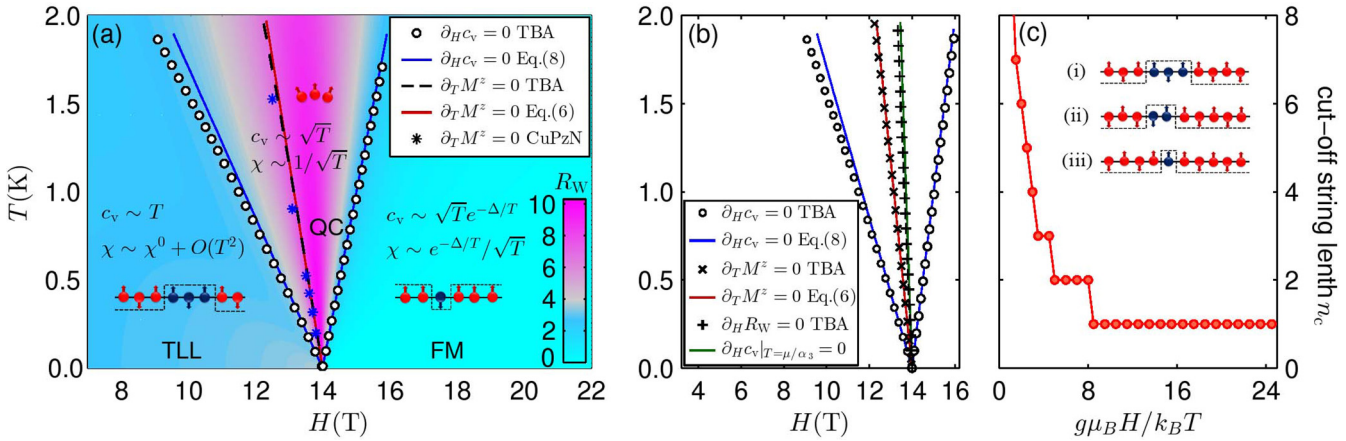

FIG. 1. (a) Contour plot of the WR in the T-H plane. Here, we used the coupling constant $2J = 10.81$ K and the Landé factor $g = 2.3$ of the spin-1/2 compound CuPzN [25]. It maps out the TLL, the quantum critical (QC), and the ferromagnetic (FM) phases. The circles fanning out from the saturation field $H_s = 4J$ show the maxima of the specific heat obtained from the TBA Eq. (3), in excellent agreement with Eq. (8) (blue solid line). The black dashed line shows the magnetization maximum determined from Eq. (3) in an agreement with the experimental data (blue stars) and Eq. (6) (red solid line) [48]. (b) The "+" symbols show the maxima of the Wilson ratio, which coincides with the minima of specific heat (dark green line). The magnetization maximum determined from Eq. (3) (the crosses) shows an agreement with the red line $T_M = \mu/\alpha_M$, with $\alpha_M = 1.3118 k_B/(g\mu_B)$ [34]. (c) The cutoff string length n_c vs the energy scale $g\mu_B H/(k_B T)$ at an accuracy of the order 10^{-6}. The cutoff n_c shows stirlike features with respect to H at low temperatures. The inset shows three schematic spin configurations: (i) $M^z = 1$ and 2 spinons; (ii) $M^z = 0$, $\nu_2 = 1$, and 2 spinons; and (iii) $M^z = 1$, $\nu_2 = 1$, and 4 spinons [34].

However, at finite temperatures and in the thermodynamic limit, there are real and complex solutions describing the different lengths of the bound states,

$$\lambda^n_{j,\ell} = \lambda^n_j + \tfrac{1}{2} i(n + 1 - 2\ell), \tag{2}$$

with $\ell = 1, \ldots, n$, and $j = 1, \ldots, \nu_n$. Here, λ^n_j and ν_n denote the real part and the number of length-n strings, respectively [2,21].

Building on such spin strings [21], the thermodynamics of the system is determined by the TBA equations

$$\varepsilon^+_n = \varepsilon^0_n - \sum_m A_{m,n} * \varepsilon^-_m(\lambda), \tag{3}$$

where $*$ denotes convolution, n takes positive integer values, and $\varepsilon^\pm_n = \pm T \ln[1 + e^{\pm\varepsilon_n/T}]$ defines the dressed energy of the length-n spin strings. The driving term is given by $\varepsilon^0_n = -2\pi J a_n(\lambda) + nH$, with the kernel function $a_n(\lambda) = \frac{1}{2\pi}\frac{n}{\lambda^2+n^2/4}$. The function $A_{m,n}$ is given in Ref. [34]. The free energy per unit length is given by $f = \sum_n \int a_n(\lambda)\varepsilon^-_n(\lambda)d\lambda$. Hereafter, all magnetic properties will be in the per unit length.

Spin strings and spin liquid. For low-lying excitations, each magnon decomposes into two spinons, i.e., spin-1/2 quasiparticles [2,35–42]. The spectral weights of two-spinon excitations have been experimentally confirmed through the observation of the spin dynamic structure factor [9–13]. In order to calculate the spin string contributions to the thermodynamics at different temperature scales, we rewrite the free energy as $f = \sum_n g_n(\lambda) + \sum_n \varepsilon^-_n(\infty)$, where $g_n = \int d\lambda\, a_n(\lambda)[\varepsilon^-_n(\lambda) - \varepsilon^-_n(\infty)]$ counts the major contribution from the length-n strings, besides their constant values $\varepsilon^\pm_n(\infty)$, to the free energy. Thus g_n is very convenient for estimating the cutoff string length n_c [34] [see Fig. 1(c)].

Here, we observe that for a small value of H/T, a large cutoff string length n_c is needed in the calculation of the thermodynamics. When $T \to \infty$, full string patterns are required, i.e., $n_c \to \infty$, so that the free energy reduces to that of free spins, $f = \sum_n \varepsilon^-_n(\infty)$. Moreover, for $H \sim 0^+$ and $T \ll 1$, logarithmic temperature corrections to the thermodynamical properties of the renormalization fixed point effective Hamiltonian have been seen [7,43,44]. At $T = 0$, all the λ_j take real values. In this case, one easily gets the known magnetization critical exponent $\delta = 2$ in the scaling form $1 - M^z/M_s = D(1 - H/H_s)^{1/\delta}$, with $D = 4/\pi$ [34]. This gives a divergent spin susceptibility at the saturation point $H_s = 4J$ [45].

For $T \ll H$, the TLL feature is dominated by the excitations close to the Fermi points of the length-1 strings ε_1. Such elementary excitations are described by particle-hole excitations. From the TBA equations (3), the dressed energy ε_1 is given by $\varepsilon_1(\lambda) = \varepsilon^{(0)}_1(\lambda) + \eta(\lambda) + O(T^3)$, where $\varepsilon^{(0)}_1(\lambda)$ is given by the dressed energy equation (3) in the limit $T = 0$ and the leading order temperature correction is determined by $\eta(\lambda) = \frac{\pi^2 T^2}{6t}[a_2(\lambda + Q) + a_2(\lambda - Q)] - a_2 * \eta(\mu)$, with $t = \frac{d\varepsilon_1(\lambda)}{d\lambda}|_{\lambda=Q}$. Here, Q is fixed by the external field through $\varepsilon^{(0)}_1(\pm Q) = 0$ (see Refs. [34,46]). For arbitrary $H < H_s$, we thus obtain the field theory result for the free energy, $f = f_0 - \pi T^2/(6v_s) + O(T^3)$, where f_0 is the ground-state energy and the sound velocity is given by $v_s = \frac{1}{2\pi}\frac{d\varepsilon_1(\lambda)/d\lambda}{\rho_0(\lambda)}|_{\lambda=Q}$ [34]. This free energy gives the relativistic behavior of phonons [4], where the specific heat is $c_v/T = \pi/(3v_s)$. This gives the dynamic critical exponent $z = 1$ [3,4,48].

Quantum criticality of spinons. In this spin-1/2 chain, the determination of the phase boundary of the TLL is still in question. In experiments [25,26], the magnetization maximum was regarded as the, as yet unjustified, TLL phase boundary [27,28]. In Figs. 1(a) and 1(b), we demonstrate that the maximum positions of the specific heat (circles) fanning out from the H_s coincide with the phase boundaries determined by

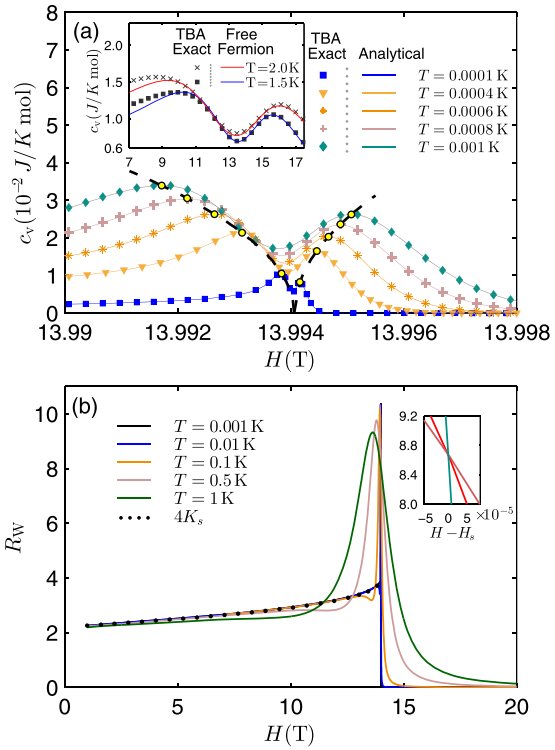

FIG. 2. (a) Numerical [symbols from (3)] and analytical [solid lines from (5)] specific heat vs magnetic field in the same setting as that of Fig. 1. The double peaks (circles) fanning out from the $H_s = 13.9941$ (T) mark the crossover temperatures separating the three regions: the TLL, the QC, and the FM (see Fig. 1). The inset shows a comparison between the results of the TBA and the free fermions [34]. (b) A numerical plot of the WR at different temperatures, which collapse to the Luttinger parameter curve of $4K_s$ calculated using (3), indicating the TLL nature. The inset shows the dimensionless scaling behavior of the WR at low temperatures.

the WR and the analytical crossover temperatures Eq. (8). The extrema of the WR and specific heat coincide with each other and thus both the WR and specific heat well capture the critical phenomenon. We observe that the magnetization maximum deviates significantly from the true TLL phase boundary as determined by the WR and the maxima in specific heat [see Fig. 1(b)]. This is mainly because the magnetization peaks almost lie in the center of the QC cone, where the susceptibility is divergent as $1/\sqrt{|H-H_s|}$. Such critical behavior was also discussed from the Grüneisen parameter [49,50], which indicates the change of spectra in the vicinity of the critical point.

Figure 2(a) shows the double-maxima structure of the specific heat, indicating energy fluctuations in three different regions: Quantum and thermal fluctuations reach an equal footing (TLL); thermal fluctuations strongly coupled to quantum fluctuation in the quantum critical (QC) region; and dilute magnons dominate the fluctuations (FM). We show that there exists an intrinsic connection between the WR and Luttinger parameter K_s for the TLL phase,

$$R_{\mathrm{W}} = 4K_s. \tag{4}$$

A similar relation was recently found in spin ladder compounds and Fermi gases [51–54]. Thus the WR elegantly quantifies the TLL regardless of the microscopic details of the underlying quantum system. This elegant relation (4) is confirmed by the numerical solutions of the TBA equations (3) [see Fig. 2(b)].

We further show that the length-1 spin strings dominate the quantum criticality of the spinons and magnons in the vicinity of the critical point [34]. We prove that the vanishing Fermi point gives rise to a universality class of free-fermion criticality, i.e., the dilute magnons. By developing the generating function of free fermions in the TBA equations (3) [34], we obtain the free energy

$$f \approx -\frac{2}{\pi}b_1 + \frac{8}{\pi}b_2 \tag{5}$$

near H_s, where $b_1 = -\frac{\sqrt{\pi}T^{\frac{3}{2}}}{4\sqrt{J}}\,\mathrm{Li}_{\frac{3}{2}}(-e^{\frac{A}{T}})$ and $b_2 = -\frac{1}{2}\frac{\sqrt{\pi}T^{\frac{5}{2}}}{(16J)^{\frac{3}{2}}}\,\mathrm{Li}_{\frac{5}{2}}(-e^{\frac{A}{T}})$, with $A = 4J - H - \frac{b_1}{\pi} + \frac{b_2}{\pi}$. This simple result gives very accurate thermal and magnetic properties for the field near the saturation field [see Fig. 2(a)]. The polylog function $\mathrm{Li}_{3/2}(x)$ appearing in b_1 indicates that dilute magnons are similar in nature to free fermions [20,27,28,48]. Here, $T \to 0$, the magnon density $n_{\mathrm{magnon}} = M_s/N - M^z = \frac{\sqrt{2m^*T}}{\pi}\int_0^\infty \frac{dx}{e^{x^2-\frac{\mu}{T}}+1}$ can be obtained from (5) in the vicinity of the critical point, where the effective mass of the magnon is given by $m^* \approx \frac{1}{2J}(1 - \frac{T^{1/2}}{\sqrt{\pi J}}\int_0^\infty \frac{dx}{e^{x^2-\frac{\mu}{T}}+1})$, with the effective chemical potential $\mu = H_s - H$. The second term in the effective mass manifests a deviation from the mass of the free fermion $m^* = 1/(2J)$ as the magnetic field moves away from the critical point [see the inset of Fig. 2(a)].

For the region beyond the TLL, i.e., $T \gg H_s - H > 0$, one can obtain entire scaling functions for the per unit length magnetization and the susceptibility,

$$M^z = \tfrac{1}{2} + \lambda_0 T^{\frac{1}{2}} f^s_{\frac{1}{2}}, \quad \chi = -\lambda_0 T^{-\frac{1}{2}} f^s_{-\frac{1}{2}}, \tag{6}$$

where $\lambda_0 = 1/(2\sqrt{\pi J})$ and $f^s_n = \mathrm{Li}_n(-e^{\frac{\mu}{T}})$. From the magnetization, we thus obtain its maximum $T_M = \mu/\alpha_M$, with $\alpha_M = 1.3118 k_B/(g\mu_B)$, which agrees with the free-fermion theory [48]. These analytical scaling functions signify the free-fermion nature of the spinons and correspond to a dynamical critical exponent $z = 2$ and a correlation length exponent $\nu = 1/2$, covering the prediction from the zero-scale factor universality hypothesis [55]. In particular, the magnetization $(M_s/N - M^z)/H \propto T^\beta$ determines the exponent $\beta = 1/2$ in the critical region. The scaling function of the specific heat in QC is given by

$$c_v = \sqrt{\frac{T}{\pi J}}\left[-\frac{3}{8}f^s_{\frac{3}{2}} + \frac{1}{2}\frac{\mu}{T}f^s_{\frac{1}{2}} - \frac{1}{2}\left(\frac{\mu}{T}\right)^2 f^s_{-\frac{1}{2}}\right]. \tag{7}$$

We see that $c_v/T \propto T^{-\alpha}$, with $\alpha = 1/2$. From the maxima of (7), we determine the two crossover temperatures for dilute magnons and spinons,

$$T_{\mathrm{magnon}} = -\frac{\mu}{\alpha_1}, \quad T_{\mathrm{spinon}} = \frac{\mu}{\alpha_2}, \tag{8}$$

whereas the specific heat dip determines the maximum value of the Wilson ratio $T_{R_W} = \mu/\alpha_3$. Here, $\alpha_{1,2,3} = y_{1,2,3}k_B/(g\mu_B)$,

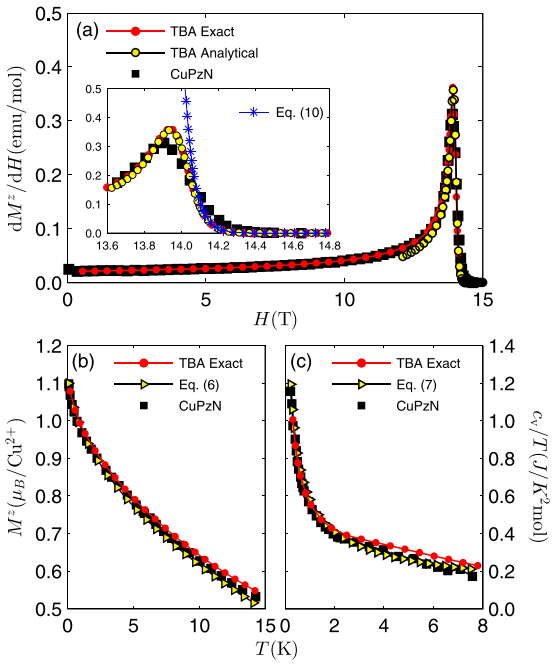

FIG. 3. (a) Susceptibility vs magnetic field at $T = 0.08$ K. The numerical [red dots (3)] and analytical [yellow triangles (5)] results agree well with the experimental measurement (black squares) for the 1D spin-1/2 antiferromagnet CuPzN [25] with the same setting used in Fig. 1. The inset shows the exponential decay of the susceptibility, as compared with Eq. (9), when the field slightly exceeds the saturation field H_s. (b) and (c) show the scaling laws of the magnetization and specific heat vs temperature, where the red dots and yellow triangles denote the numerical TBA (3) result and the analytical scalings Eqs. (6) and (7), which agree well with the experimental data (black squares).

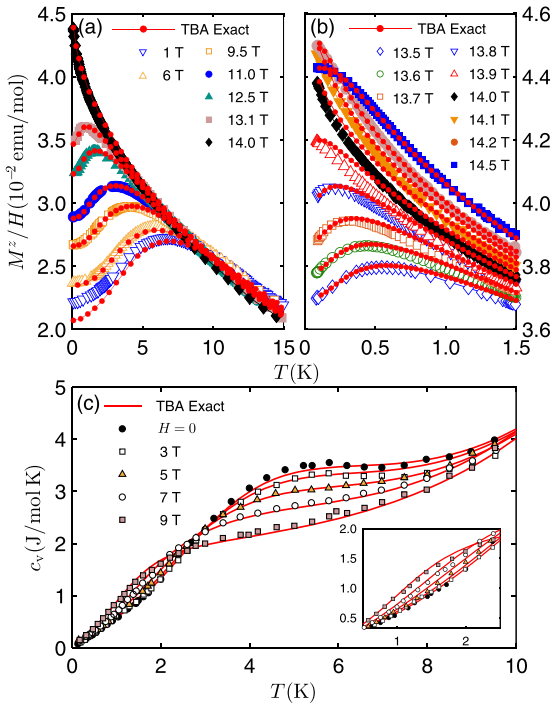

FIG. 4. (a) Experimental magnetization M^z/H vs temperature at various fields (symbols) for the antiferromagnet CuPzN [25]. The red dots show the TBA numerical result with the same setting used in Fig. 1. For the case $H = 1.0$ T, we considered $n = 120$ spin strings in order to reach a stable numerical accuracy. (b) shows the magnetization for low temperatures ($T \leqslant 1.5$ K) and for magnetic fields near H_s, comparing the numerical result (red dots) with the experimental data (symbols). (c) Specific heat vs temperature for CuPzN [35] with different magnetic fields. The symbols and solid red lines stand for the experimental and TBA numerical results from (3) with the cutoff string $n_c = 30$. Here, the phonon contribution is included. The inset shows the linear T-dependent signature within the curves as $T \to 0$.

with $y_1 = 1.5629$, $y_2 = 3.6205$, and $y_3 = 0.4284$, which agree quite well with the numerical TBA result (see Fig. 1). The two crossover temperatures (8) are also valid for the 1D Bose gas [56]. For $H \gtrsim H_s$, the ferromagnetic ordering leads to a gapped phase where the susceptibility decays exponentially,

$$\chi = \frac{1}{2\sqrt{\pi JT}} e^{-\Delta_g/T}, \quad \Delta_g = 4J - H, \tag{9}$$

illustrating the universal behavior of the dilute magnons [see Fig. 3(a)].

By definition, the WR in the critical region satisfies the scaling behavior $R_W \approx (\frac{4\pi k_B}{3g\mu_B})^2 f^s_{-1/2}/f^s_{3/2}$ as $H \to H_s$. It follows that the WR curves at low temperatures intersect, where the slopes are proportional to $1/T$ [see the inset of Fig. 2(b)]. So far, we have analytically obtained all critical exponents in QC,

$$\alpha = \beta = 1/2, \quad \delta = 2, \quad z = 2, \quad \nu = \tfrac{1}{2}. \tag{10}$$

They satisfy the pronounced relation $\alpha + \beta(1 + \delta) = 2$.

Application to the spin material. The analytical results obtained here for the quantum scaling functions (6)–(10) provide a precise understanding of the quantum criticality of the ideal spin-1/2 antiferromagnet CuPzN [25], on which high-precision measurements of the thermal magnetic properties have been made. Here, the best fit of magnetic properties determines the coupling constant $2J = 10.81$ K, Landé factor $g = 2.3$, and the saturation field $H_s = 13.9941$ (T) which only slightly differ from the experimental values $2J = 10.8(1)$ K, $g = 2.3(1)$, and $H_s = 13.97(6)$ (T), respectively. Figure 3(a) shows excellent agreement between our theoretical results for the susceptibility and the experimental data for the CuPzN in the measured region. In particular, one can identify dilute magnon behavior for magnetic fields exceeding H_s [see the inset of Fig. 3(a)]. Indeed, the scaling forms of the susceptibility (6) and specific heat (7) fit quite well with the experimental data [see Figs. 3(b) and 3(c)]. However, we mention a small discrepancy between the theoretical result and experimental data for the susceptibility in a narrow window around the critical point. This is due to a three-dimensional (3D) coupling effect, which has also been noted in spin ladder compounds [26,57,58].

In Figs. 4(a) and 4(b), we have compared our theoretical calculations with experimental measurements for the magnetization of the CuPzN subjected to both weak and strong magnetic fields. There was no theoretical examination on the magnetization data measured in this experiment [25]. Although there is overall agreement between our results and the data, an obvious discrepancy between theory and

experiment was observed for $H \sim J'$ or $H_s - H \sim J'$ due to 3D interchain coupling. For this model, $J' \approx 0.046$ K [see the magnetization curves at $H = 14.0, 13.9, 13.8$ T in Fig. 4(b)]. In addition, by properly choosing the cutoff string n_c, we can analyze the full thermodynamics of the model in the entire temperature regime by solving the TBA equation (3). Figure 4(c) shows an excellent agreement between the TBA result and experimental data for the specific heat.

Acknowledgments. The authors thank T. Giamarchi, D. Ridout, and H. Pu for helpful discussions. This work is supported by the NSFC under Grant No. 11374331, the Key NSFC Grant No. 11534014, and the National Key R&D Program of China Grant No. 2017YFA0304500. H.-Q.L. acknowledges financial support from NSAF U1530401 and computational resources from the Beijing Computational Science Research Centre.

[1] C. N. Yang and C. P. Yang, Phys. Rev. **150**, 321 (1966); **150**, 327 (1966); **151**, 258 (1966).
[2] L. D. Faddeev and L. A. Takhtajan, Phys. Lett. A **85**, 375 (1981).
[3] F. D. M. Haldane, Phys. Rev. Lett. **47**, 1840 (1981).
[4] I. Affleck, Phys. Rev. Lett. **56**, 2763 (1986).
[5] M. Takahashi, *Thermodynamics of One-Dimensional Solvable Models* (Cambridge University Press, Cambridge, UK, 1999).
[6] Y. Wang, W.-L. Yang, J. Cao, and K. Shi, *Off-Diagonal Bethe Ansatz for Exactly Solvable Models* (Springer, Berlin, 2015).
[7] D. C. Johnston, R. K. Kremer, M. Troyer, X. Wang, A. Klümper, S. L. Budko, A. F. Panchula, and P. C. Canfield, Phys. Rev. B **61**, 9558 (2000).
[8] D. A. Tennant, R. A. Cowley, S. E. Nagler, and A. M. Tsvelik, Phys. Rev. B **52**, 13368 (1995).
[9] B. Lake, D. A. Tennant, C. D. Frost, and S. E. Nagler, Nat. Mater. **4**, 329 (2005).
[10] M. Mourigal, M. Enderle, A. Klöpperpieper, J.-S. Caux, A. Stunault, and H. M. Rønnow, Nat. Phys. **9**, 435 (2013).
[11] B. Lake, D. A. Tennant, J.-S. Caux, T. Barthel, U. Schollwock, S. E. Nagler, and C. D. Frost, Phys. Rev. Lett. **111**, 137205 (2013).
[12] A. Zheludev, V. O. Garlea, L.-P. Regnault, H. Manaka, A. Tsvelik, and J.-H. Chung, Phys. Rev. Lett. **100**, 157204 (2008).
[13] M. B. Stone, D. H. Reich, C. Broholm, K. Lefmann, C. Rischel, C. P. Landee, and M. M. Turnbull, Phys. Rev. Lett. **91**, 037205 (2003).
[14] I. Affleck, Phys. Rev. Lett. **56**, 746 (1986).
[15] J. Cardy, Nucl. Phys. B **270**, 186 (1986).
[16] T. Giamarchi, *Quantum Physics in One Dimension* (Oxford University Press, Oxford, UK, 2004).
[17] F. H. L. Essler, H. Frahm, A. R. Its, and V. E. Korepin, J. Phys. A **29**, 5619 (1996).
[18] V. E. Korepin, N. M. Bogoliubov, and A. G. Izergin, *Quantum Inverse Scattering Method and Correlation Functions* (Cambridge University Press, Cambridge, UK, 1993).
[19] F. H. L. Essler, H. Frahm, F. Göhmann, A. Klümper, and V. E. Korepin, *The One-Dimensional Hubbard Model* (Cambridge University Press, Cambridge, UK, 2005).
[20] H. J. Schulz, Phys. Rev. B **22**, 5274 (1980).
[21] M. Takahashi, Prog. Theor. Phys. **46**, 401 (1971).
[22] C. N. Yang and C. P. Yang, J. Math. Phys. (NY) **10**, 1115 (1969).
[23] A. Sommerfeld, Z. Phys. **47**, 1 (1928).
[24] K. G. Wilson, Rev. Mod. Phys. **47**, 773 (1975).
[25] Y. Kono, T. Sakakibara, C. P. Aoyama, C. Hotta, M. M. Turnbull, C. P. Landee, and Y. Takano, Phys. Rev. Lett. **114**, 037202 (2015).
[26] Ch. Rüegg, K. Kiefer, B. Thielemann, D. F. McMorrow, V. Zapf, B. Normand, M. B. Zvonarev, P. Bouillot, C. Kollath, T. Giamarchi, S. Capponi, D. Poilblanc, D. Biner, and K. W. Krämer, Phys. Rev. Lett. **101**, 247202 (2008).
[27] V. R. Shaginyan, V. A. Stephanovich, K. G. Popov, E. V. Kirichenko, and S. A. Artamonov, Ann. Phys. (Berlin) **528**, 483 (2016).
[28] M. Jeong and H. M. Rønnow, Phys. Rev. B **92**, 180409(R) (2015).
[29] A. H. van Amerongen, J. J. P. van Es, P. Wicke, K. V. Kheruntsyan, and N. J. van Druten, Phys. Rev. Lett. **100**, 090402 (2008).
[30] Y. Liao, A. S. C. Rittner, T. Paprotta, W. Li, G. B. Partridge, R. G. Hulet, S. K. Baur, and E. J. Mueller, Nature (London) **467**, 567 (2010).
[31] M. Boll, T. A. Hilker, G. Salomon, A. Omran, J. N. L. Pollet, I. Bloch, and C. Gross, Science **353**, 1257 (2016).
[32] A. Iaizzi, K. Damle, and A. W. Sandvik, Phys. Rev. B **95**, 174436 (2017).
[33] H. A. Bethe, Z. Phys. **71**, 205 (1931).
[34] See Supplemental Material at http://link.aps.org/supplemental/10.1103/PhysRevB.96.220401 for details of the calculation of the main results given in this Rapid Communication.
[35] P. R. Hammar, M. B. Stone, D. H. Reich, C. Broholm, P. J. Gibson, M. M. Turnbull, C. P. Landee, and M. Oshikawa, Phys. Rev. B **59**, 1008 (1999).
[36] M. Karbach and G. Müller, Phys. Rev. B **62**, 14871 (2000).
[37] M. Karbach, D. Biegel, and G. Müller, Phys. Rev. B **66**, 054405 (2002).
[38] J.-S. Caux, R. Hagemans, and J.-M. Maillet, J. Stat. Mech. (2005) P09003.
[39] J.-S. Caux and R. Hagemans, J. Stat. Mech. (2006) P12013.
[40] M. Kohno, Phys. Rev. Lett. **102**, 037203 (2009).
[41] A. Klauser, J. Mosset, and J.-S. Caux, J. Stat. Mech. (2012) P03012.
[42] W. Yang, J. Wu, S. Xu, Z. Wang, and C.-J. Wu, arXiv:1702.01854.
[43] S. Lukyanov, Nucl. Phys. B **522**, 533 (1998).
[44] S. Eggert, I. Affleck, and M. Takahashi, Phys. Rev. Lett. **73**, 332 (1994).
[45] J. C. Bonner and M. E. Fisher, Phys. Rev. **135**, A640 (1964).
[46] For $T < H \sim 0^+$ the free energy has been calculated by the Wiener-Hopf method [47].
[47] L. Mezincescu and R. I. Nepomechie, in *Quantum Groups, Integrable Models and Statistical Systems*, edited by J. LeTourneux and L. Vinet (World Scientific, Singapore, 1993), pp. 168–191; L. Mezincescu, R. I. Nepomechie, P. K. Townsend, and A. M. Tsvelik, Nucl. Phys. B **406**, 681 (1993).

[48] Y. Maeda, C. Hotta, and M. Oshikawa, Phys. Rev. Lett. **99**, 057205 (2007).

[49] M. Garst and A. Rosch, Phys. Rev. B **72**, 205129 (2005).

[50] D. Strassel, P. Kopietz, and S. Eggert, Phys. Rev. B **91**, 134406 (2015).

[51] K. Ninios, T. Hong, T. Manabe, C. Hotta, S. N. Herringer, M. M. Turnbull, C. P. Landee, Y. Takano, and H. B. Chan, Phys. Rev. Lett. **108**, 097201 (2012).

[52] X.-W. Guan, X.-G. Yin, A. Foerster, M. T. Batchelor, C.-H. Lee, and H.-Q. Lin, Phys. Rev. Lett. **111**, 130401 (2013).

[53] Y.-C. Yu, Y.-Y. Chen, H.-Q. Lin, R. A. Römer, and X.-W. Guan, Phys. Rev. B **94**, 195129 (2016).

[54] Z. Saghafi, J. Jahangiri, S. Mahdavifar, H. Hadipour, and S. Farjami Shayesteh, J. Magn. Magn. Mater. **398**, 183 (2016).

[55] S. Sachdev, T. Senthil, and R. Shankar, Phys. Rev. B **50**, 258 (1994).

[56] B. Yang, Y.-Y. Chen, Y.-G. Zheng, H. Sun, H.-N. Dai, X.-W. Guan, Z.-S. Yuan, and J.-W. Pan, Phys. Rev. Lett. **119**, 165701 (2017).

[57] M. Klanjšek, H. Mayaffre, C. Berthier, M. Horvatic, B. Chiari, O. Piovesana, P. Bouillot, C. Kollath, E. Orignac, R. Citro, and T. Giamarchi, Phys. Rev. Lett. **101**, 137207 (2008).

[58] B. Thielemann, C. Rüegg, H. M. Rønnow, A. M. Läuchli, J.-S. Caux, B. Normand, D. Biner, K. W. Krämer, H.-U. Güdel, J. Stahn, K. Habicht, K. Kiefer, M. Boehm, D. F. McMorrow, and J. Mesot, Phys. Rev. Lett. **102**, 107204 (2009).